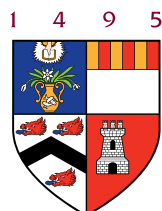


Analyzing Wind Patterns on Mars across different Martian Seasons

Anurag A. Chaudhari

A dissertation submitted in partial fulfilment
of the requirements for the degree of
Master of Science in Data Science
of the
University of Aberdeen.



Department of Physics

16-08-2024

Declaration

No portion of the work contained in this document has been submitted in support of an application for a degree or qualification of this or any other university or other institution of learning. All verbatim extracts have been distinguished by quotation marks, and all sources of information have been specifically acknowledged.

Signed: Anurag Avinash Chaudhari

Date: 16-08-2024

Abstract

This study explores wind patterns on Mars by applying Correlation Image Velocimetry (CIV) on ultraviolet images captured by the EXI instrument onboard the EMM spacecraft. The primary objective was to plot wind fields over a large region of Mars and analyze their seasonal variations. To improve the accuracy of the wind field vector extraction, histogram equalization was applied to enhance contrast before processing images with CIV. The enhancement intensified cloud structures in the images making identification of the movement between frames more precise and ultimately leading to clearer wind field calculation. Following image enhancement and CIV processing, the study revealed wind patterns to be following the Hadley circulation.

This research establishes a method for extracting large-scale wind data from planetary images, with significant potential for future atmospheric research. This opens opportunities for refining image processing techniques to increase the accuracy further. The study contributes to a deeper understanding of Martian wind behaviour, providing valuable information for scientific inquiry and future exploration missions.

Acknowledgements

I would like to express my deepest gratitude to my supervisor, Dr. Roland Young, for his invaluable guidance, support, and encouragement throughout the course of my research. His expertise and insightful feedback have been instrumental in shaping this work, and I am truly grateful for the time and effort he invested in helping me develop both my ideas and my skills.

I would also like to extend my thanks to my colleagues and friends for their encouragement, as well as my family for their unwavering support and patience during this journey.

Finally, I am thankful to the entire research community and the institutions that have provided the resources and opportunities necessary to complete this thesis.

Contents

| | | |
|----------|---|-----------|
| 1 | Introduction | 6 |
| 1.1 | Problem Statement | 6 |
| 1.2 | Literature Review | 6 |
| 1.2.1 | Mars Clouds | 7 |
| 1.2.2 | Martian Winds and Changes in Wind Pattern | 7 |
| 1.2.3 | Correlation Image Velocimetry | 7 |
| 2 | Dataset | 9 |
| 2.1 | EMM | 9 |
| 2.2 | EXI | 9 |
| 3 | Methods | 12 |
| 3.1 | Image Processing | 12 |
| 3.1.1 | Region selection | 12 |
| 3.1.2 | Histogram Equalization | 12 |
| 3.2 | Cloud tracking | 13 |
| 3.2.1 | CIV | 13 |
| 3.2.2 | Optimizing Parameters | 14 |
| 3.3 | Calculating windspeed | 14 |
| 4 | Results and Discussion | 16 |
| 4.1 | Wind fields | 16 |
| 4.1.1 | Wind Direction | 16 |
| 4.1.2 | Wind Speed | 21 |
| 5 | Conclusion | 26 |

Chapter 1

Introduction

Mars has always been an area of interest for a lot of scientists for years now because of its similarity to Earth. Its shape, axial tilt, and elliptical orbit roughly resemble our Earth and researchers think that study on Mars can give us an idea about Earth's future. The Martian atmosphere provides crucial insights into Earth's possible atmospheric evolution (Forget et al., 2013). These studies might one day help humankind to terraform the planet Mars and make it habitable (Zubrin and Wagner, 1996). As humans try to explore Mars more and more, knowledge of Martian winds could prove to be essential to facilitate this research. Knowing Martian winds can help us make better decisions about what possible challenges our missions could face in landing spacecraft safely, designing habitats and using wind as a power source to fuel research there on the surface of Mars (Martínez et al., 2017; Guzewich et al., 2021; Viúdez-Moreiras et al., 2022).

But how do we measure something that is not visible like air? This has been an issue even on Earth. One of the most logical ways to measure wind would be to track something that floats in the atmosphere, like clouds. In this thesis, I have tracked Martian clouds as pictured by the EXI instrument onboard the Emirates Mars Mission (EMM) using the Correlation Image velocimetry (CIV) method. I have used the UV images captured by this instrument as they highlight cloud structure better than the visible wavelength images. Here, I am studying changes in wind patterns according to different Mars seasons and drawing logical comparisons to previous studies about Hadley circulation on Mars.

1.1 Problem Statement

Measuring wind is a challenge even on Earth. The first satellite to measure wind speeds by the direct motion of the air molecules using a Doppler shift phenomenon known as Light Detection and Ranging (LiDAR) was launched quite recently, in 2018 (Lux et al., 2020). Devices like anemometers can indicate local wind speed at that moment, but to plot a large-scale general circulation picture of wind structure, using satellite imaging is very important. Tracking the motion of the clouds over a known time interval helps us plot wind patterns covering a large range of latitudes and longitudes on Mars. We can use these plots to compare changes in the general circulation of wind with changes in the Martian Season.

1.2 Literature Review

The “Red Planet”, Mars, is considered as the closest analogue to Earth in our solar system. Could Mars be humankind's future abode? Can the Martian atmosphere help us predict the future of

Earth? Exploring the Martian atmosphere could help us find these answers. The martian atmosphere is significantly thinner than Earth. It is primarily composed of carbon dioxide, nitrogen, argon, and small amounts of oxygen and water vapour. The atmospheric ice column contained in clouds consists of mainly two components, carbon dioxide and water ice (Clancy et al., 2017; Scholten et al., 2010). Due to low atmospheric pressure and temperature on Mars, water vapour exists as ice rather than liquid water vapour in clouds.

1.2.1 Mars Clouds

The position of Mars relative to the Sun or Mars Season (L_S) has a significant influence on water cloud activity in the Martian atmosphere. Cloud activity is most prominent in the aphelion season, that is, in Mars Season (L_S) 0° - 180° . Based on their latitudes, these clouds are classified into two categories, polar hoods (Benson et al., 2011) and the Aphelion Cloud Belt (ACB) between -10° to 30° latitude range. In this project, we focus on ACB whose three phases based on the season are the formation phase, peak phase around $L_S = 75^\circ$, and decaying phase (Guha et al., 2021). These Martian clouds during cloud season are usually found between 15 to 30 km altitude ((Campbell et al., 2020)).

1.2.2 Martian Winds and Changes in Wind Pattern

Mars has large seasonal changes due to its highly eccentric orbit. This change has a significant effect on the circulation of winds on Mars. To measure Martian winds, scientists have employed various methods and devices, both on the surface and from the orbit. The Mars Orbit Camera onboard the Mars Global Surveyor has studied wind patterns through cloud tracking and the wind patterns across large areas in the polar regions of Mars (Wang and Ingersoll, 2003). Synoptic-scale images of Mars captured by the Hubble Space Telescope have also been used previously (Mischna et al., 1998). These images are used to track clouds and calculate wind speed.

Much like that on Earth, Martian general circulation also shows circulation cells in each hemisphere. The air moves towards the equator at lower latitudes and rises vertically due to high temperatures. At higher altitudes, the wind moves polewards to form a circulation cell called the Hadley cell. The magnitude of circulation in each hemisphere depends on the season and position of Mars relative to the Sun. Both the hemispheres show symmetrical cells during the Vernal and Autumnal Equinox. During both Winter and Summer Solstices will have one Hadley cell that crosses the equator, air rising in the summer hemisphere and descending in the winter hemisphere. The span of such a single Hadley cell can be around 90° latitudes on Mars (Lewis and Holmes, 2021). Figure 1 shows the diagram of Mean meridional circulation that indicates Hadley cell in four different Martian Seasons.

1.2.3 Correlation Image Velocimetry

Correlation Image Velocimetry is a tool used to track the motion of fluids in various scientific fields. We have used this method here to track the motion of clouds to further calculate wind direction and speed. In this method correlation algorithms are applied to a pair of images to measure displacement of features such as clouds. The CIV method has been previously used to study wind patterns on Saturn by using the images taken by the Cassini spacecraft. By tracking the motion of clouds over time, scientists were able to study the vertical and horizontal wind shear in Saturn's atmosphere (Liu et al., 2019). CIV was also used to study the Great Red Spot and other

storms in Jupiter's atmosphere using images from the Cassini mission (Choi et al., 2007).

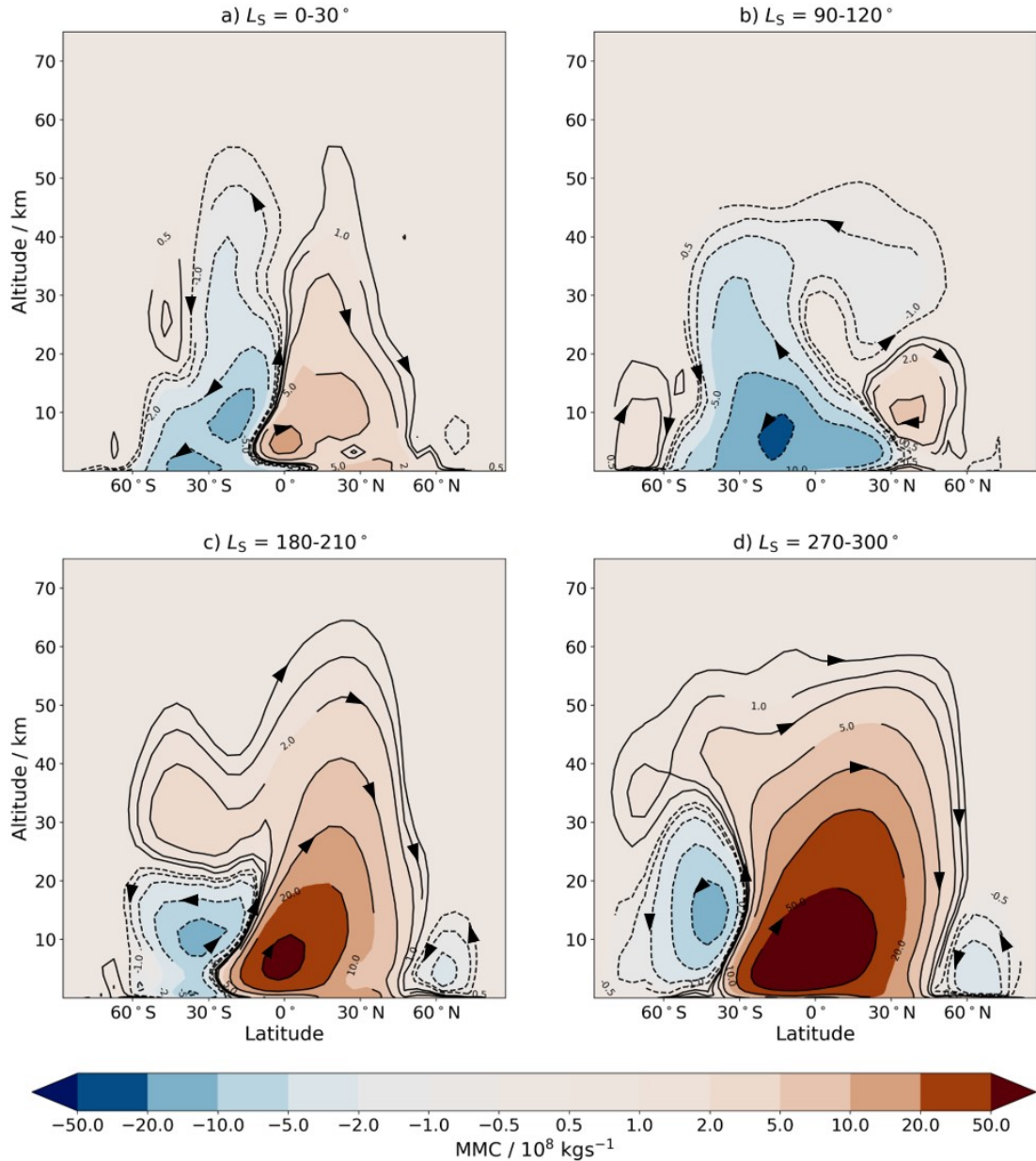


Figure 1: Mean meridional circulation (MMC) patterns showing Hadley Cells at four different seasons during Mars Year (MY) 30 in the OpenMARS database (Lewis and Holmes, 2021).

Chapter 2

Dataset

2.1 EMM

The Hope Probe, which is part of the Emirates Mars Mission (EMM) was launched by United Arab Emirates to study the Martian atmosphere. The goals of EMM include understanding the climate of Mars and investigating the connection between current Martian weather and the ancient climate of Mars, explaining the loss of Hydrogen and Oxygen into space, as mentioned on the EMM Science Data Center (SDC) website (URL: <https://emiratesmarsmission.ae>). EMM probe has three instruments onboard (Figure 2), Emirates eXploration Imager (EXI), Emirates Mars InfraRed Spectrometer (EMRS), and Emirates Mars Ultraviolet Spectrometer (EMUS).



Figure 2: EMM instruments onboard Hope probe (Jones et al., 2021)

2.2 EXI

EXI instrument (Figure 3) operates on six wavelengths, 220, 260, 320, 437, 546 and 635 nm using two telescopes, ultraviolet (UV) and visible (VIS). 437, 546 and 635 nm are the visible (VIS) range

wavelengths, while 220, 260, 320 nm fall under ultraviolet (UV) range filters. Visible images show the surface features and atmospheric elements like dust storms and cloud formations. Whereas, the UV images focus on the distribution of ozone and water ice clouds by showing higher contrast between cloud structure and surface.

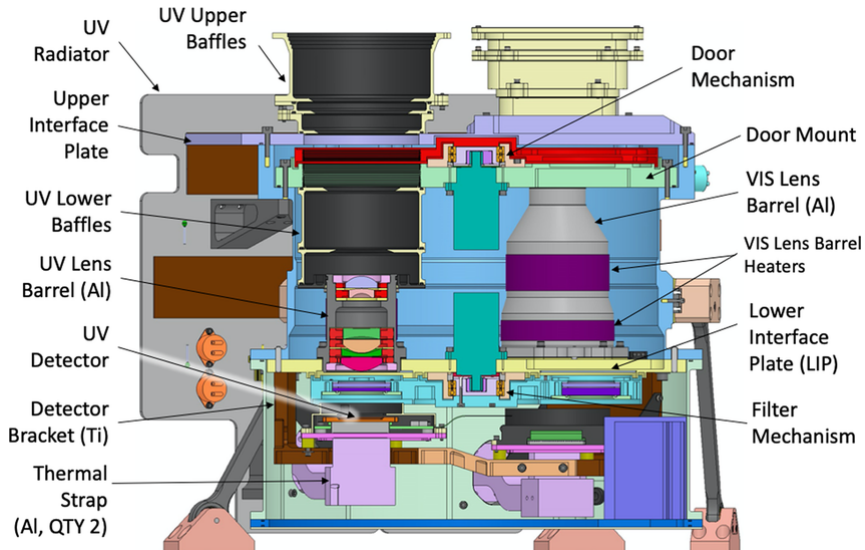


Figure 3: EXI Sensor Head (Jones et al., 2021)

Each EXI image is of 3072 X 4095 pixels (Jepesen et al., 2022). The orbit of the Hope Probe is elliptical, so the surface distance corresponding to each pixel varies from 2 to 4 kilometers depending on the position of the spacecraft (Jones et al., 2021). EXI instrument has several observation sets XOS1, XOS2, XOS4, XOS5, XOS6, XOS7, each with different objective and strategy. XOS1 and XOS2 images have lower resolution. XOS2 provides observations of areas EMIRS cannot capture in XOS1. XOS4 is a medium resolution image taken once a week, while XOS5 is for calibration. XOS6 is mostly used for dust analysis. For this project, we will use the XOS7 images which are taken over short time intervals allowing for accurate cloud motion measurements.

Out of the three UV wavelengths, we have used 320 nm images because these show a higher contrast between clouds and surface, and are highly effective for detecting clouds. The primary reason for this is the scattering and reflection of UV light by the water ice clouds. Hence the clouds appear brighter in these images, allowing for clear identification from the background. EXI images are of primarily 3 levels based on the extent of processing: Level 1 (L1), Level 2A (L2A) (Figure 4) which is the image of Mars captured by the EXI instrument, Level 2B (L2B) which is an L2A image projected on an equirectangular projection, and Level 3. We have used 3 sets of L2B point-corrected images, each set in a different Martian Season, to compare the velocity fields. L2B images are further processed to minimize the jitter effect caused by slight movements of the spacecraft due to instability, to produce L2B point corrected images. Table 1 presents details regarding the image sequences we have used in our study.

| | Earth Date | UTC | | Time separation (min) | L_S (°) | Mars Year | Number of images |
|------------|------------|----------|----------|-----------------------|-----------|-----------|------------------|
| Sequence 1 | 2021-11-22 | 14:16:52 | 14:56:52 | 5 | 131 | MY36 | 9 |
| Sequence 2 | 2022-12-28 | 09:55:51 | 10:55:57 | 30 | 1 | MY37 | 3 |
| Sequence 3 | 2023-06-10 | 18:43:46 | 19:43:52 | 30 | 76 | MY37 | 3 |

Table 1: Sequences of images used in this thesis.

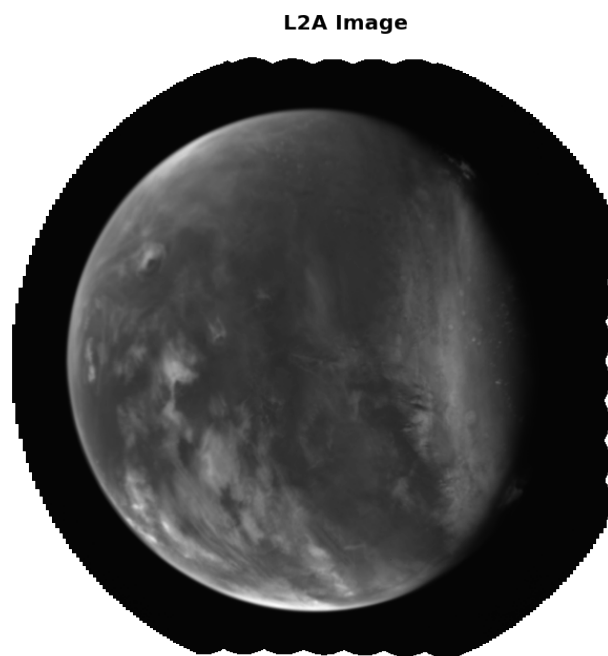


Figure 4: Level 2A (L2A) image in Sequence 1, UTC: 2021-11-22 14:16:52. The South pole region of Mars can be seen towards the right in the image

Chapter 3

Methods

3.1 Image Processing

3.1.1 Region selection

We have used point-corrected Level 2B (L2B) (Figure 5) images for our study. These images are L2A images projected on an equirectangular grid. Then certain post-processing is done to reduce the jitter effect, which is called point correction. Initially, we plotted L2B image data in Jupyter Notebook to get an L2B image. We have to convert the pixels into latitudes and longitudes as explained later in this thesis. Then we cropped a rectangular section between latitudes: -30° to 30° , to focus on the equatorial clouds and longitudes: -150° to -70° , to avoid any edges in each of the three sequences.

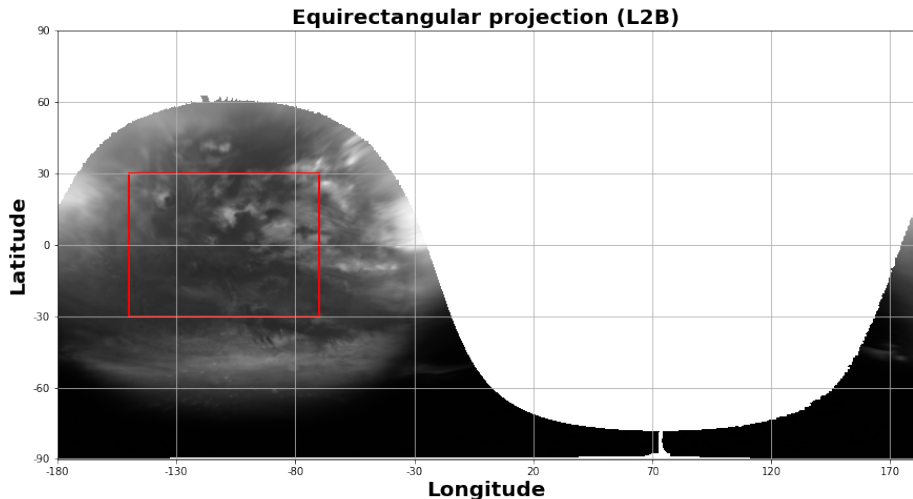


Figure 5: Level 2B (L2B) point corrected image showing equirectangular projection of L2A image in Figure 4. The red rectangular box shows the region selected for the study in this thesis.

3.1.2 Histogram Equalization

We applied the Histogram Equalization method to enhance the visibility of moving features. This method is based on mapping the original distribution to another wider and more uniformly distributed distribution so that the intensity values are spread over the entire range. First, the Cumulative Distribution Function (CDF) is calculated as follows:

$$H'(i) = \sum_{0 \leq j < i} H(j)$$

Where $H(i)$ is the frequency value at an intensity in the original histogram and $H'(i)$ its cumulative distribution. Then the cumulative distribution is normalized such that the maximum value is 255.

Then a simple re-mapping procedure is used to obtain the intensity values of the equalized image:

$$\text{equalized}(x,y) = H'(\text{src}(x,y))$$

Here, $\text{equalized}(x,y)$ represents the new intensity value at (x,y) , $\text{src}(x,y)$ is the original intensity value at (x,y)

However, the transformed image showed huge distortion towards the extremes of the image histogram, which could lead to a loss of details. We adjusted the extent of histogram equalization such that it does not compress the image histogram towards extremes. We blended the original image and the transformed image in a ratio of 3:2 to get the controlled equalized image. Figure 6 shows the images and their image histograms.

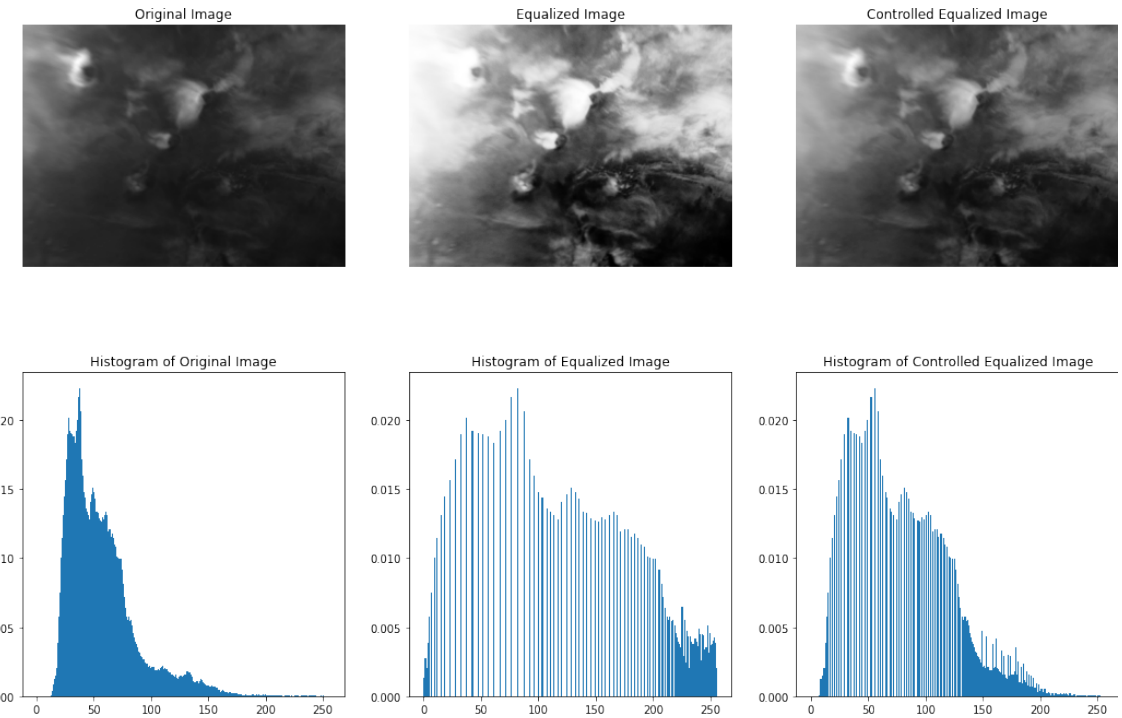


Figure 6: Image Transformation using controlled histogram equalization. The image here is from Sequence 3, UTC: 2023-05-06 18:51:36.

3.2 Cloud tracking

3.2.1 CIV

Correlation Image Velocimetry is used to measure the motion of the clouds and calculate the wind speed. It is a function provided inside the Universal Velocity and MATerial Transport (UVMAT) toolbox hosted in MATrix LABoratory (MATLAB). CIV uses a pattern-matching technique as

shown in Figure 7, to detect cross-correlation between two image pairs taking into account the deformation of cloud shape.

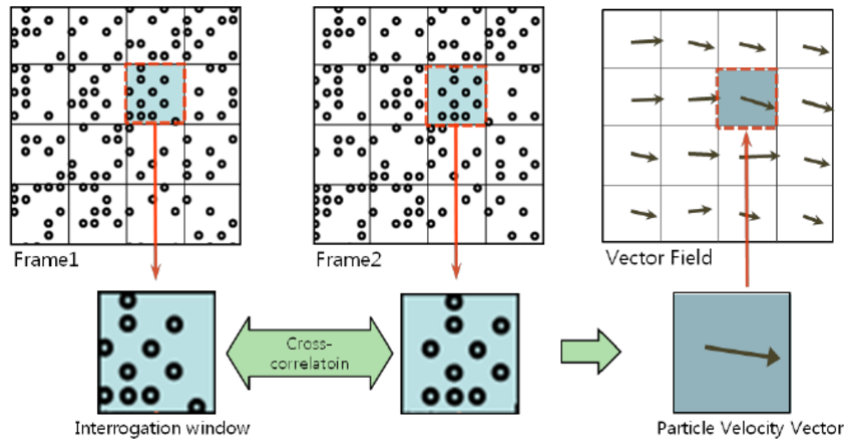


Figure 7: Diagram displaying the CIV technique (Choi et al., 2011)

3.2.2 Optimizing Parameters

Numerous parameters need to be optimized to obtain an accurate CIV measurement, mostly by deploying trial and error method. The time interval between the image pairs needs to be chosen appropriately such that it is large enough for the motion to be detected and avoid having vectors incorrectly ignored. But if it is too long, the algorithm will not be able to differentiate between deformation and movement and might display false vectors. Therefore, the time separation must be small enough to provide good correlation but large enough to provide good accuracy.

The size of the correlation box should be big enough to fit major cloud structures. The difference between the sizes of the search box and correlation box must allow for the movement of clouds in that time interval. For each image pair, the CIV algorithm was applied twice with different sets of parameters for finer measurements. CIV1: For the first sequence, the correlation box size and the search box size were 81 X 81 pixels and 90 X 90 pixels respectively. Whereas for the second and third sequences, they were 81 X 81 pixels and 111 X 111 pixels respectively. For the second and third sets of images, the time interval was 30 minutes, so the difference between their sizes was increased to detect more range of motion. Some filters were applied to remove vectors with a correlation of less than 0.2 and vectors near the edge of the search box. Then the velocity field was interpolated using the thin plane spline method on a regular grid with field smooth parameter kept at 10.

For CIV2: for sequence 1 the correlation box was reduced to 71 X 71 pixels and the search box was reduced to 75 X 75 pixels. For the other two sequences, 71 X 71 and 85 X 85 respectively. The same filters as CIV1 were also applied in CIV2 but with a field smooth parameter at 2.

3.3 Calculating windspeed

An important step in this project was to convert the pixels into latitudes and longitudes. The data received in the L2B file is in units of pixels and we need to re-label the image in order to display latitudes and longitudes of that region. This is crucial so that further calculations of

cloud displacement can be obtained in units of degrees and can be converted to units of kilometers considering the curvature of the planet. Hence it was necessary to establish a relation between x and y coordinates of the image and corresponding latitudes and longitudes. The equations are as follows:

$$\text{longitude} = \lambda_W + (\lambda_E - \lambda_W) \frac{x_{\text{CIV}}}{\eta_x}$$

$$\text{latitude} = \phi_S + (\phi_N - \phi_S) \frac{y_{\text{CIV}}}{\eta_y}$$

Where λ_E and λ_W are the west and eastern most longitudes, ϕ_N and ϕ_S are north and south latitudes, x is pixel location in x -axis and y is pixel location in y -axis. While, η_x are the total number of pixels in x -direction and η_y are the the total number of pixels in y -direcion.

After conducting CIV, the values of u -direction and v -direction are in units of pixels, where u -direction is displacement in x -direction and v -direction is in y -direction. Curvature of Mars needs to be taken into account before calculating wind speed. Now to calculate wind speed in kilometers per hour, we used these equations:

$$v_x = \frac{u}{\Delta t} \frac{\lambda_E - \lambda_W}{\Delta x} \frac{\pi}{180} r \cos(\phi)$$

$$v_y = \frac{v}{\Delta t} \frac{\phi_N - \phi_S}{\Delta y} \frac{\pi}{180} r$$

Here, v_x and v_y are the wind velocities in x and y direction respectively, and $\Delta x, \Delta y$ are changes in longitudes and latitudes in degrees per pixel, respectively. r is the radius of Mars approximately 3389.5 kilometers. Δt is the time interval between two images. Δt is $\frac{1}{6}$ hours for Sequence 1 and $\frac{1}{2}$ hours for second and third sequence.

Total longitudes in the region of study are 80° and latitudes are 60° . The dimension of the extracted image is 1280 X 960 pixels. Hence, $\Delta x, \Delta y$ can be calculated as:

$$\Delta x = \frac{80}{1280} = 0.0625$$

$$\Delta y = \frac{60}{960} = 0.0625$$

To calculate the extent of our region of study in kilometers:

$$L = 2\pi r * \frac{80}{360} \approx 9465.27 \text{ km}$$

$$B = \pi r * \frac{60}{180} \approx 3549.47 \text{ km}$$

Here, L is the length of the region of study in x -direction along the equator and B is the breadth across the latitude range in y -direction.

Chapter 4

Results and Discussion

4.1 Wind fields

Wind fields display wind patterns at different latitudes and longitudes, which helps to generate a general sense of wind direction and speed. Here we have compared wind field plots of three sequences taken in different Mars seasons, across the same latitudinal and longitudinal range. We have drawn comparisons based on two factors: Wind direction and Wind Speed.

4.1.1 Wind Direction

In this section, I have presented the field plots obtained after conducting CIV measurements on each of the three sets. In each of the plots, the colour and the corresponding direction are: red is east, blue is west, yellow is north, and green is south. The length of each vector represents the magnitude of wind speed.

Our first sequence ($L_S = 131^\circ$) (Figure 8) has nine images that span over a total of 40 minutes. For CIV measurements I used four pairs of images, each separated by 10 minutes. These wind fields are obtained in aphelion season, ($L_S = 0$ to 140°), hence the cloud density and consequently, wind field vector density is lower than in other sequences. A west-bound belt is consistent in each of these four plots, near the equator (between -10° to 0° degrees latitudes). An east/northeast moving wind pattern can be observed in the latitude range -20° to -10° and longitudes -115° to -75° .

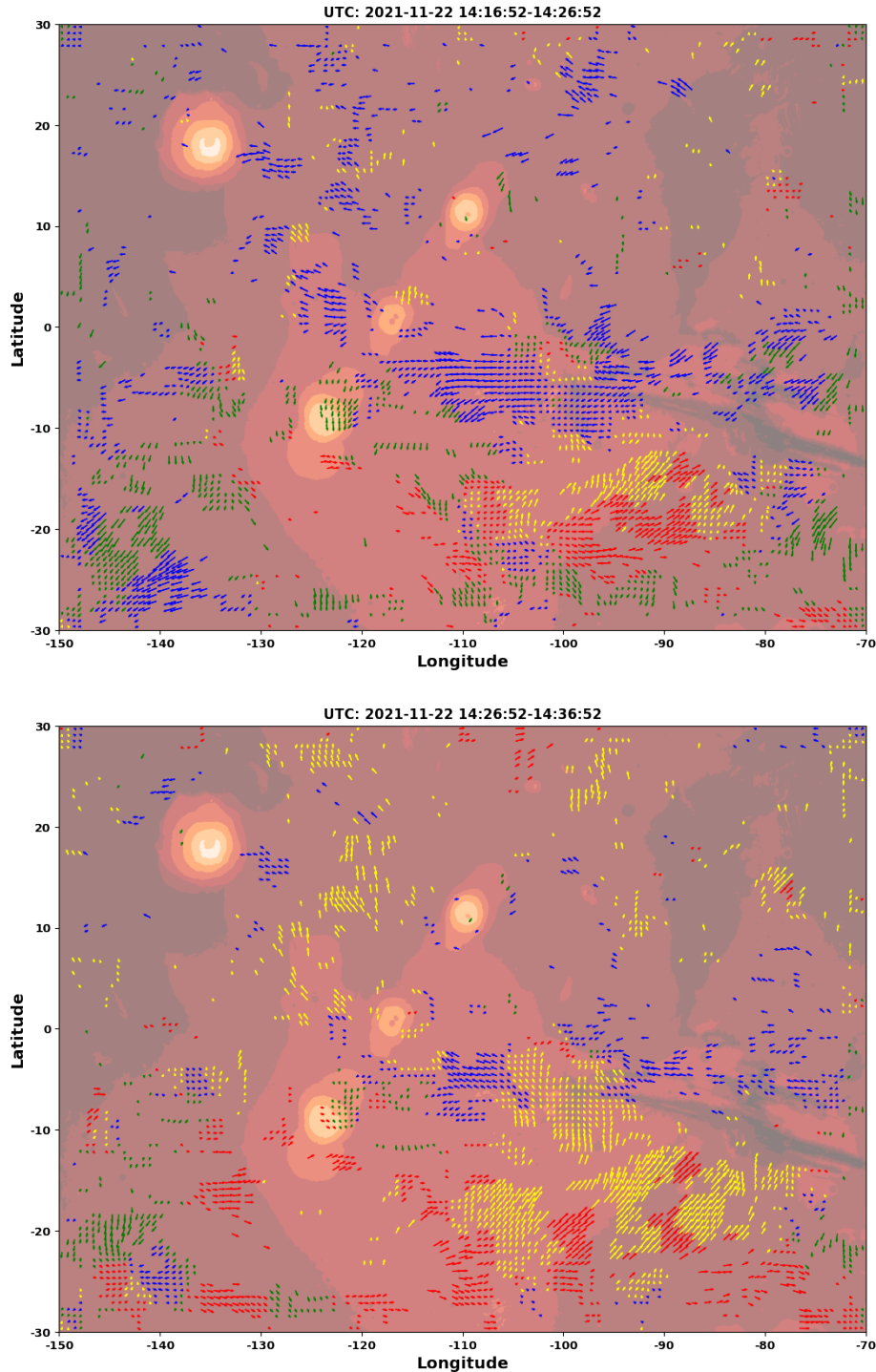


Figure 8: Wind Direction plot: Sequence 1 ($L_S = 131^\circ$). Blue: towards west, Red: east, Green: south, Yellow: north. The brown shade contours represent the topography of Mars using MOLA topography data.

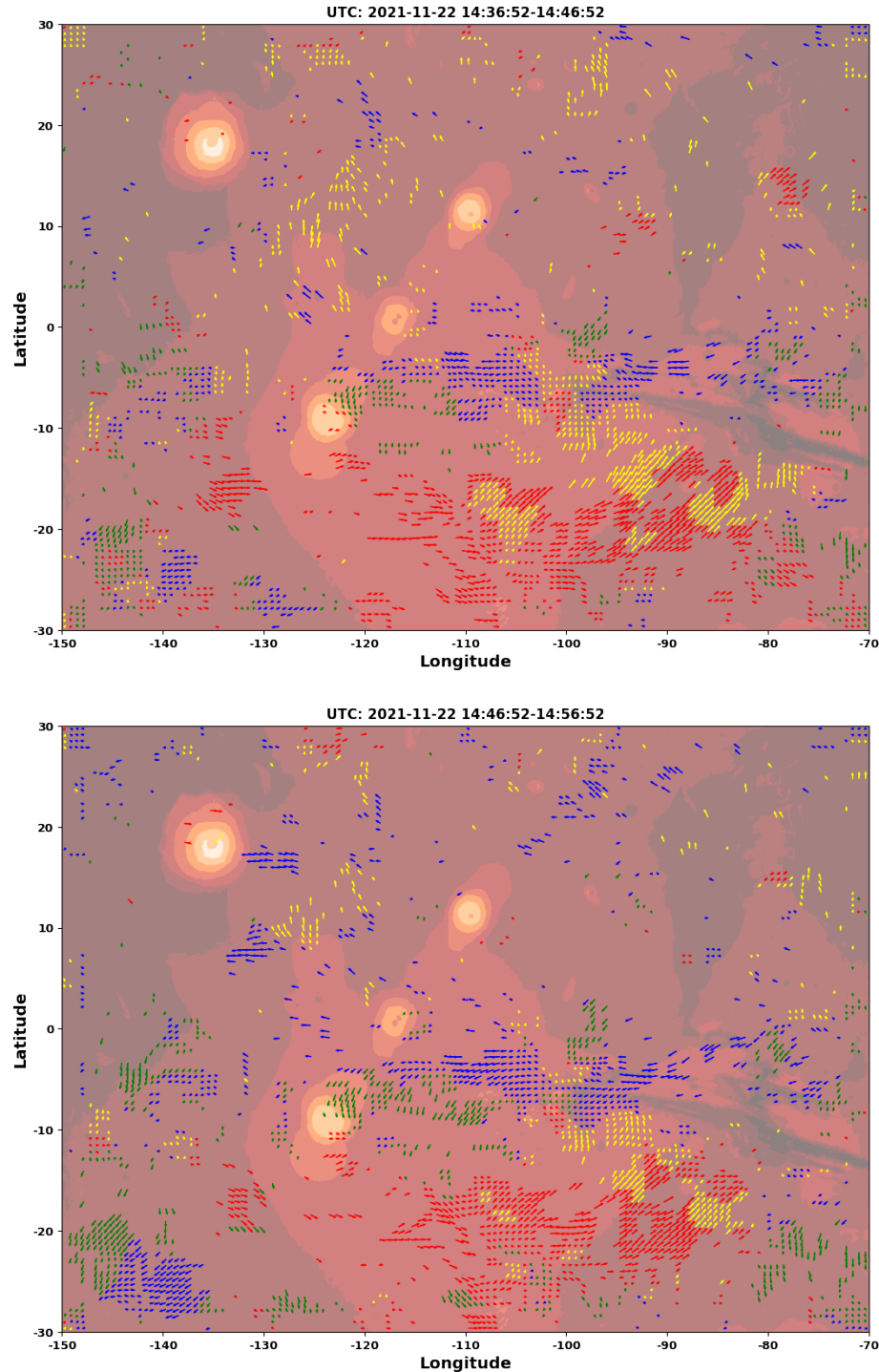


Figure 8: Wind Direction plot: Sequence 1 ($L_S = 131^\circ$). Blue: towards west, Red: east, Green: south, Yellow: north. The brown shade contours represent the topography of Mars using MOLA topography data. (continued)

In the second set of images ($L_S = 1^\circ$) (Figure 9), wind vectors away from the equator can be seen in both hemispheres. Strong wind between latitudes 10° to 20° degrees and longitude -115° to -105° southward pattern. There's northward wind between latitudes -130° to -70° and between longitude ranges 0 to 20 degrees. While in the southern hemisphere, a southward moving pattern can be seen between -100° to -80° degrees in the longitude range and between latitudes 0° to -20° .

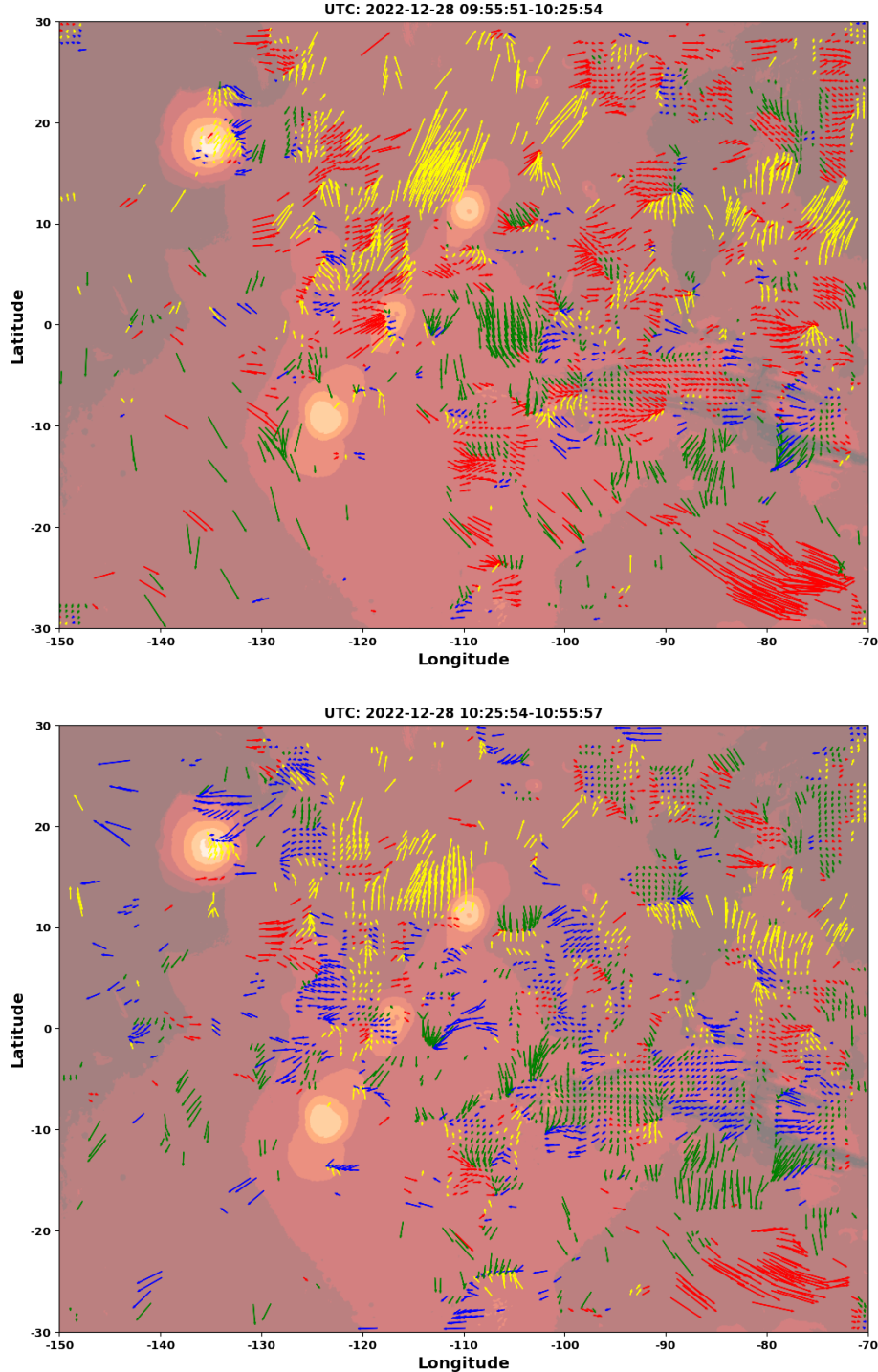


Figure 9: Wind Direction plot: Sequence 2 ($L_S = 1^\circ$). Otherwise like Figure 8

The third sequence $L_S = 76^\circ$ (Figure 10) shows a weak westward belt near the equator. The northern hemisphere has a general wind movement towards the west while the southern hemisphere shows a general wind direction towards the northeast. However, wind patterns seem to cross over the equator from the southern hemisphere to the northern hemisphere as indicated by yellow vectors between -10° to 10° latitudes.

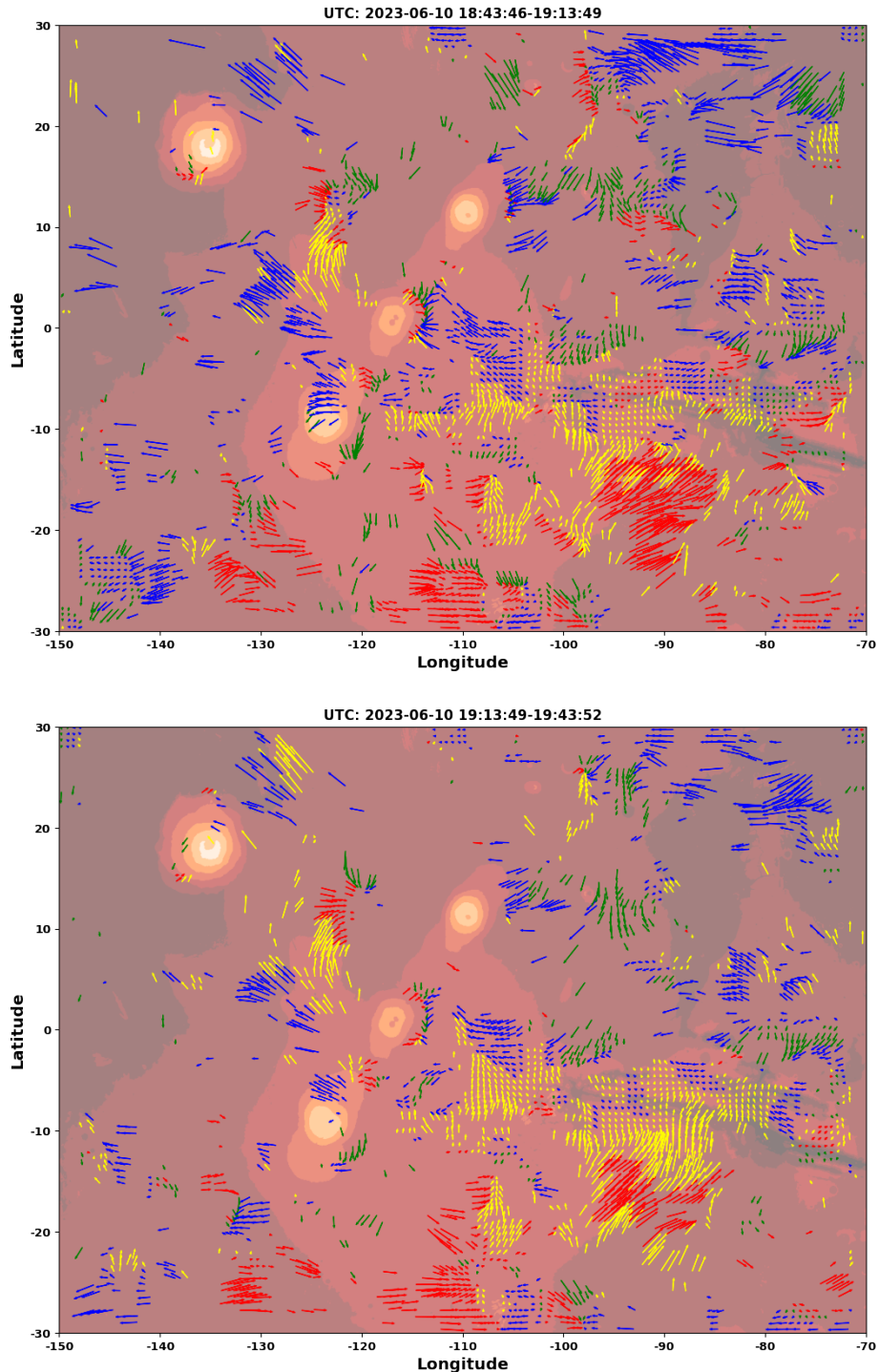


Figure 10: Wind Direction plot: Sequence 3 ($L_S = 76^\circ$). Otherwise like Figure 8

4.1.2 Wind Speed

Here we will try to analyze the wind speeds. Green vector indicates wind speed below 30 km/hr, blue is between 30 to 80 km/hr, and red vectors are above 80 km/hr.

In the sequence 1 (Figure 11), the belt near the equator (between -10° to 0° degrees latitudes) shows mostly blue vectors in all 4 images and on an average moderate speed. The east/northeast moving wind pattern in the latitude range -20° to -10° and longitudes -115° to -75° occasionally shows high speed vectors in red.

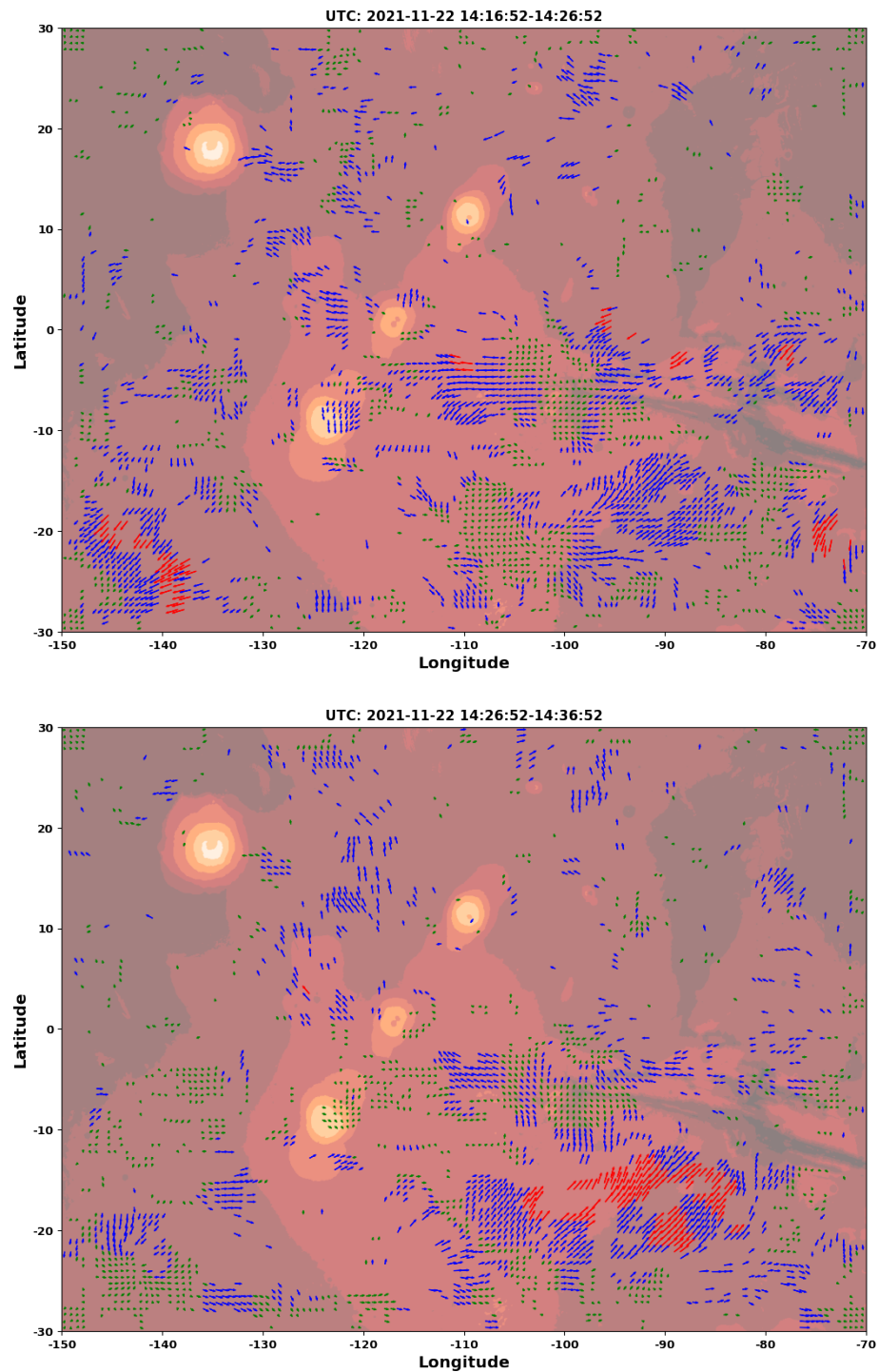


Figure 11: Wind Speed plot: Sequence 1 ($L_S = 131^\circ$). Green: below 30 km/hr, Blue: 30 - 80 km/hr, Red: more than 80 km/hr. The brown shade contours represent the topography of Mars using MOLA topography data.

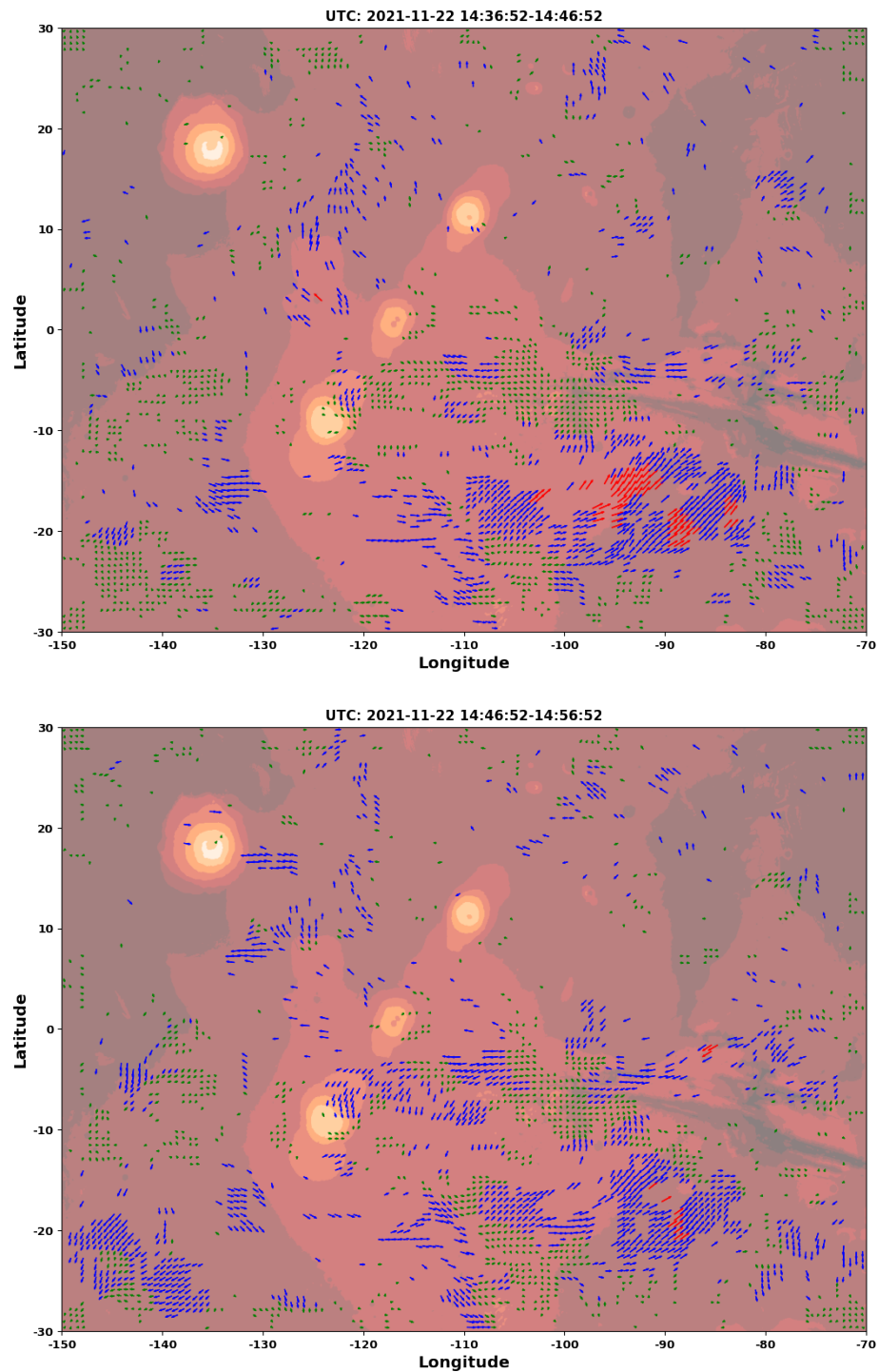


Figure 11: Wind Speed plot: Sequence 1 ($L_S = 131^\circ$). Green: below 30 km/hr, Blue: 30 - 80 km/hr, Red: more than 80 km/hr. The brown shade contours represent the topography of Mars using MOLA topography data. (continued)

In the second sequence ($L_S = 1^\circ$) (Figure 12), wind pattern between latitudes 10° to 20° degrees and longitude -115° to -105° does exhibit red vectors during first 30 minutes. Moderate to low speed winds towards the north can be observed near the equator in the northern hemisphere, and southwards in the southern hemisphere, between -100° to -80° longitude and between latitudes 0° to -20° . High speed wind fields can be observed towards the right bottom corner between latitudes -80° to -70° latitudes.

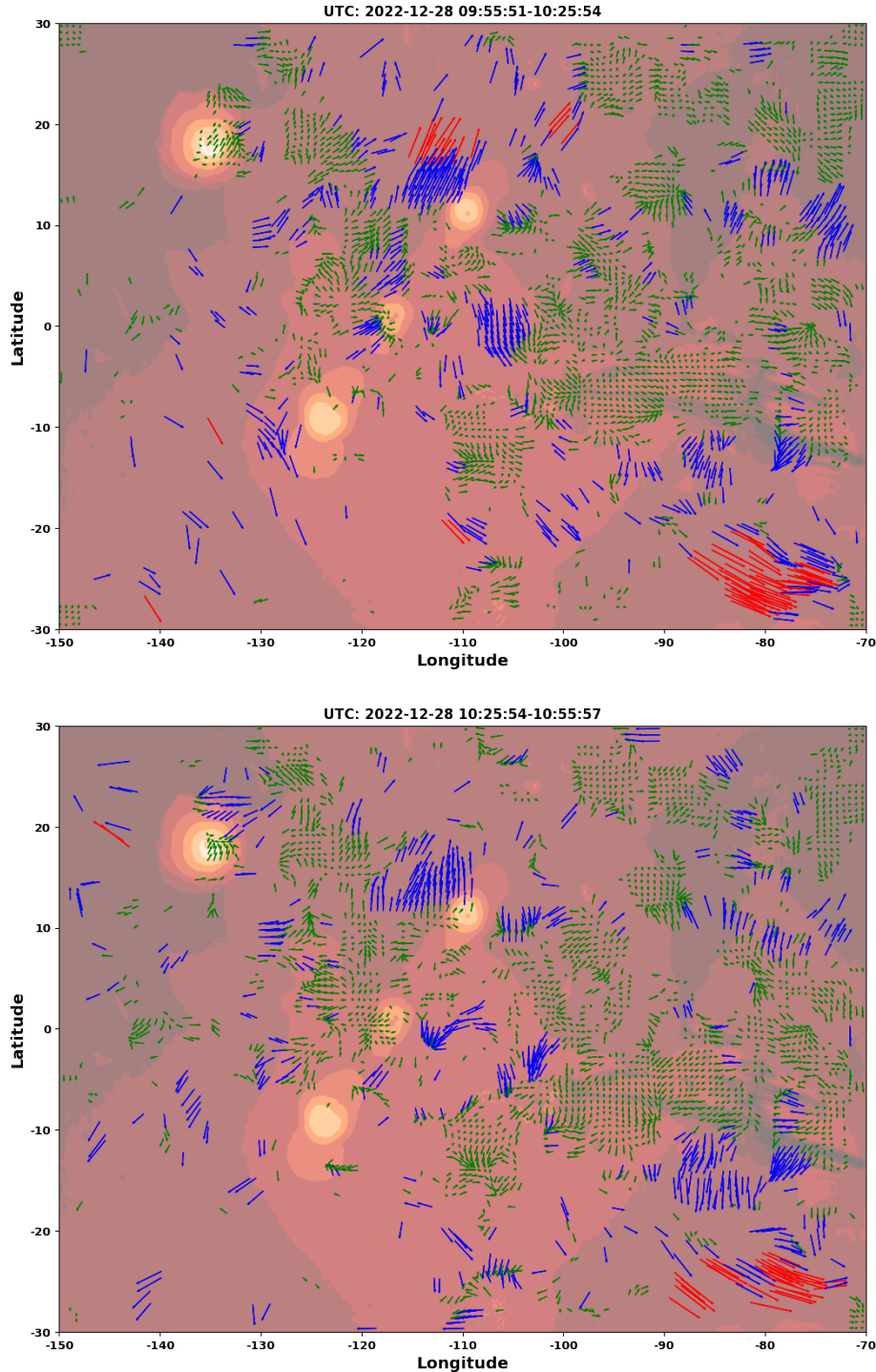


Figure 12: Wind Speed plot: Sequence 2 ($L_S = 1^\circ$). Otherwise like Figure 11

The third sequence $L_S = 76^\circ$ (Figure 13) shows a low speed westward belt near the equator. Moderate wind speed vector cluster can be observed between latitudes: -25° to -10° and longitudes: -100° to -85° pointed towards the northeast. Low speed wind vectors cross over the equator from the southern hemisphere to the northern hemisphere between -10° to 10° latitudes.

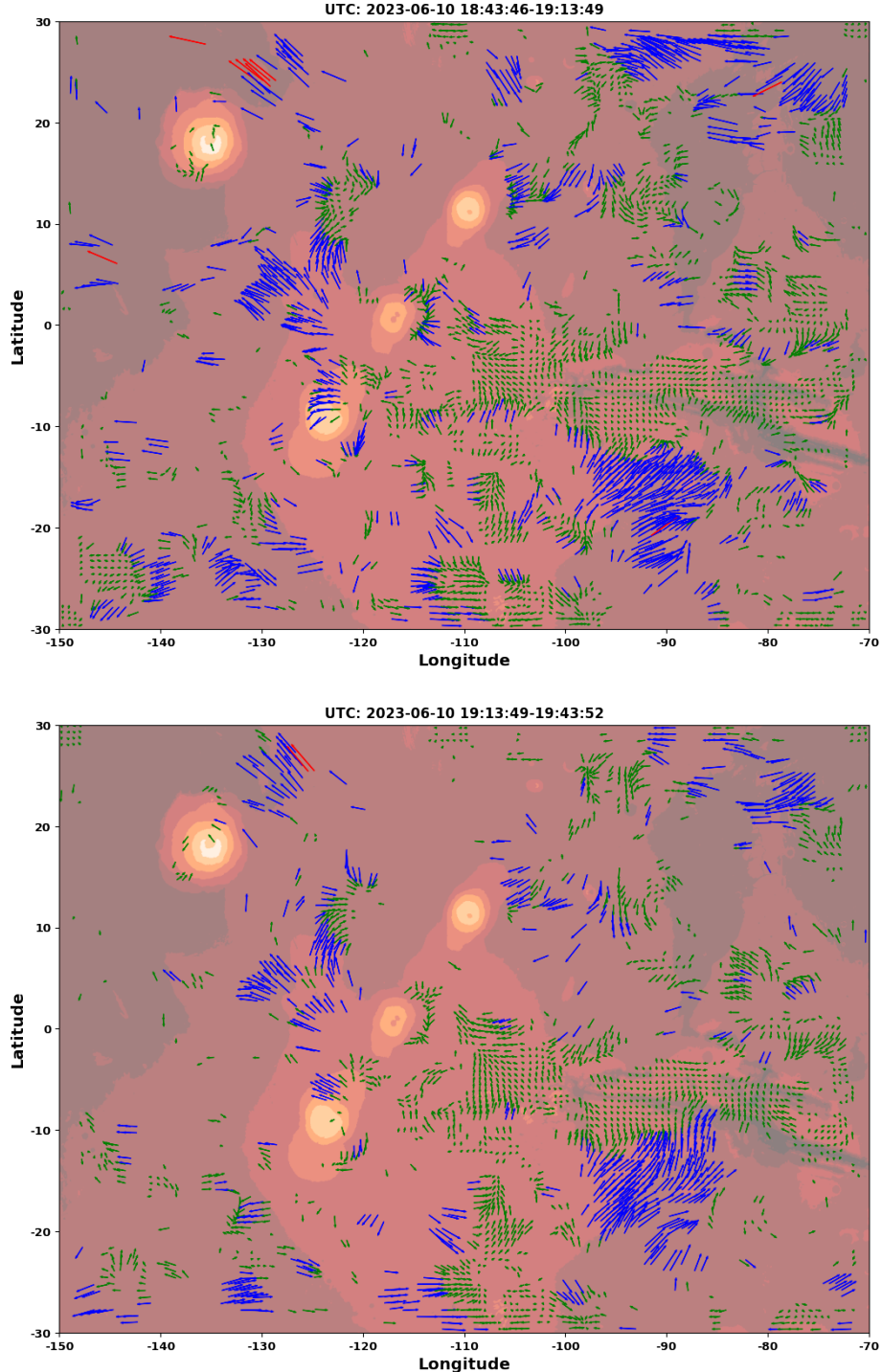


Figure 13: Wind Speed plot: Sequence 3 ($L_S = 76^\circ$). Otherwise like Figure 11

Chapter 5

Conclusion

The study aims to enhance understanding of Martian wind patterns by tracking cloud motion using the CIV method on the UV images captured by the EXI instrument onboard the EMM spacecraft. The findings from this research contribute to gaining valuable insights into the seasonal variation of wind patterns on Mars. This holds significance in understanding the history of Mars, and potentially the future of the Earth, and provides valuable knowledge for future explorations.

Through the analysis of UV images from the EXI instrument, this study successfully mapped the wind fields in a large-scale region of Mars. The study revealed the presence of wind patterns matching the description of the Hadley circulation on Mars. Sequence 2 ($L_s = 1^\circ$) shows wind motion away from the equator as expected in Hadley circulation. Even in sequence 3 ($L_s = 76^\circ$), wind patterns can be seen crossing the equator from the southern hemisphere to the northern hemisphere and following the Hadley circulation. Hence our findings align with previous studies, validating the CIV method as a reliable tool for studying Martian atmospheric dynamics.

However, there are challenges in extracting accurate vectors in certain regions. Less contrast between cloud structure and background makes it difficult to get vectors in that region. Hence, the effectiveness of the contrast-enhancing technique plays an important role. Uncertainty also arises due to pixel size, which can cause inaccuracies in calculated velocities.

This study's approach can serve as a foundation for a more detailed analysis of Martian winds using this dataset as well as future Martian explorations. The findings offer clues about Mars' climatic history and its atmospheric evolution. Moving forward, this work can be expanded to explore more detailed atmospheric models and to refine the CIV technique further helping us to gain even more detailed insights into dynamic Martian atmosphere.

Bibliography

- Benson, J. L., Kass, D. M., and Kleinböhl, A. (2011). Mars' north polar hood as observed by the Mars Climate Sounder. *Journal of Geophysical Research*, 116:E03008.
- Campbell, C. L., Kling, A. M., Guzewich, S. D., Smith, C. L., Kloos, J. L., Lemmon, M. T., Moore, C. A., Cooper, B. A., Haberle, R. M., and Moores, J. E. (2020). Estimating the altitudes of Martian water-ice clouds above the Mars Science Laboratory rover landing site. *Planetary and Space Science*, 182:104785.
- Choi, D., Banfield, D., Gierasch, P., and Showman, A. (2007). Velocity and Vorticity Measurements of Jupiter's Great Red Spot Using Automated Cloud Feature Tracking. *Icarus*, 188:35–46.
- Choi, S. M., Kim, W. H., Côté, D., Park, C.-W., and Lee, H. (2011). Blood cell assisted in vivo Particle Image Velocimetry using the confocal laser scanning microscope. *Optics Express*, 19:4357.
- Clancy, R. T., Montmessin, F., Benson, J., Daerden, F., Colaprete, A., and Wolff, M. J. (2017). *Mars Clouds*, pages 76–105. Cambridge University Press.
- Forget, F., Wordsworth, R., Millour, E., Madeleine, J.-B., Kerber, L., Leconte, J., Marcq, E., and Haberle, R. (2013). 3D modelling of the early Martian climate under a denser CO_2 atmosphere: Temperatures and CO_2 ice clouds. *Icarus*, 222:81–99.
- Guha, B. K., Panda, J., and Wu, Z. (2021). Observation of Aphelion Cloud Belt over Martian Tropics, Its Evolution, and Associated Dust Distribution from MCS Data. *Advances in Space Research*, 67:1392–1411.
- Guzewich, S. D., Abshire, J. B., Baker, M. M., Battalio, J. M., Bertrand, T., Brown, A. J., Colaprete, A., Cook, A. M., Cremons, D. R., Crismani, M. M., Dave, A. I., Day, M., Desjean, M.-C., Elrod, M., Fenton, L. K., Fisher, J., Gordley, L. L., Hayne, P. O., Heavens, N. G., Hollingsworth, J. L., Jha, D., Jha, V., Kahre, M. A., Khayat, A. S. J., Kling, A. M., Lewis, S. R., Marshall, B. T., Martínez, G., Montabone, L., Mischna, M. A., Newman, C. E., Pankine, O. A., Riris, H., Shirley, J. H., Smith, M. D., Spiga, A., Sun, X., Tamppari, L. K., Young, R. M. B., Viúdez-Moreiras, D., Villanueva, G. L., Wolff, M. J., and Wilson, R. J. (2021). Measuring mars atmospheric winds from orbit. *Bulletin of the American Astronomical Society*, 53(4). Whitepaper submitted to the Planetary Science and Astrobiology Decadal Survey 2023-2032.
- Jeppesen, C., Jones, A., Shuping, R., and Wolff, M. (2022). EXI Data Product Guide. Retrieved February 2023.
- Jones, A. R., Wolff, M., Alshamsi, M., Osterloo, M., Bay, P., Brennan, N., Bryant, K., Castleman, Z., Curtin, A., DeVito, E., Drake, V. A., Ebuen, D., Espejo, J., Farren, J., Fenton, B., Fisher, C., Fisher, M., Fortier, K., Gerwig, S., Heberlein, B., Jeppesen, C., Khoory, M. A., Knappmiller,

- S., Knavel, J., Koski, K., Looney, K., Lujan, P., Miller, M., Newcomb, G., Otzinger, G., Passe, H., Pilinski, E., Reed, H., Shuping, R., Sicken, P., Summers, D., Wade, S., Walton, L., and Yaptengco, J. L. (2021). The Emirates Exploration Imager (EXI) Instrument on the Emirates Mars Mission (EMM) Hope Mission. *Space Science Reviews*, 217:81.
- Lewis, S. and Holmes, J. (2021). Martian meteorology. *Royal Meteorological Society*. Accessed: 2024-08-15.
- Liu, T., Sayanagi, K. M., Brueshaber, S. R., Blalock, J. J., Ingersoll, A. P., Dyudina, U. A., and Ewald, S. P. (2019). Saturn's North Polar Vortex Structure Extracted From Cloud Images by the Optical Flow Method. *Journal of Geophysical Research: Planets*, 124:3041–3062.
- Lux, O., Lemmerz, C., Weiler, F., Marksteiner, U., Witschas, B., Rahm, S., Geiß, A., and Reitebuch, O. (2020). Intercomparison of wind observations from the European Space Agency's Aeolus satellite mission and the ALADIN Airborne Demonstrator. *Atmospheric Measurement Techniques*, 13:2075–2097.
- Martínez, G. M., Newman, C. N., Vicente-Retortillo, A. D., Fischer, E., Renno, N. O., Richardson, M. I., Fairén, A. G., Genzer, M., Guzewich, S. D., Haberle, R. M., Harri, A.-M., Kemppinen, O., Lemmon, M. T., Smith, M. D., de la Torre-Juárez, M., and Vasavada, A. R. (2017). The Modern Near-Surface Martian Climate: A Review of In-situ Meteorological Data from Viking to Curiosity. *Space Science Reviews*, 212:295–338.
- Mischna, M. A., Bell, J. F., James, P. B., and Crisp, D. (1998). Synoptic measurements of Martian winds using the Hubble Space Telescope. *Geophysical Research Letters*, 25:611–614.
- Scholten, F., Hoffmann, H., Määttänen, A., Montmessin, F., Gondet, B., and Hauber, E. (2010). Concatenation of HRSC colour and OMEGA data for the determination and 3D-parameterization of high-altitude CO₂ clouds in the Martian atmosphere. *Planetary and Space Science*, 58:1207–1214.
- Viúdez-Moreiras, D., de la Torre, M., Gómez-Elvira, J., Lorenz, R. D., Apéstigue, V., Guzewich, S., Mischna, M., Sullivan, R., Herkenhoff, K., Toledo, D., Lemmon, M., Smith, M., Newman, C. E., Sánchez-Lavega, A., Rodríguez-Manfredi, J. A., Richardson, M., Hueso, R., Harri, A. M., Tamppari, L., Arruego, I., and Bell, J. (2022). Winds at the Mars 2020 Landing Site. 2. Wind Variability and Turbulence. *Journal of Geophysical Research: Planets*, 127.
- Wang, H. and Ingersoll, A. P. (2003). Cloud-tracked winds for the first Mars Global Surveyor mapping year. *Journal of Geophysical Research: Planets*, 108.
- Zubrin, R. and Wagner, R. (1996). *The case for Mars: the plan to settle the red planet and why we must*. The Free Press. Accessed: 03 August 2024, via National Library of Australia.